Octave-Spanning Supercontinuum Generation in As2S3-Silica Hybrid Waveguides Pumped by Thulium-Doped Fiber Laser

Vasilii Voropaev, Shangran Xie, Aleksandr Donodin, Daniil Batov, Mikhail Tarabrin, Johann Troles, Vladimir Lazarev

Octave-Spanning Supercontinuum Generation in As_2S_3-Silica Hybrid Waveguides Pumped by Thulium-Doped Fiber Laser

Vasilii Voropaev, Shangran Xie, Aleksandr Donodin, Daniil Batov, Mikhail Tarabrin, Johann Troles, and Vladimir Lazarev

***Abstract*—Broadband supercontinuum sources are of interest for various applications. The near-infrared region (1-3 μm) is specifically useful for biomedical diagnostics. One of the promising media for supercontinuum generation in the infrared region is the strongly guiding nonlinear waveguide with an arsenic trisulfide core (As_2S_3) and a fused silica cladding. The geometrical and chemical properties of such a waveguide allow to finely tune the dispersion landscape and nonlinearity through the core diameter variations. Here we report the generation of octave-spanning supercontinuum in As_2S_3-silica hybrid nanospike waveguides pumped by a thulium-doped all-fiber femtosecond laser and amplifier system at 1.9 μm wavelength. The widest supercontinuum was obtained in the wavelength range from 1.1 to 2.5 μm (full width at -10 dB) in the waveguide with a core diameter of 1.7 μm. Generation of significant dispersive waves, as well as third harmonics component, is observed. Numerical simulation shows that the generated supercontinua are coherent in the entire spectral range and can be exploited to create a self-referenced laser comb.**

***Index Terms*—Chalcogenide, thulium-doped fiber lasers, nanospike, supercontinuum generation.**

Manuscript received 15 September 2022; revised 24 January 2023; accepted 22 February 2023. Date of publication 8 March 2023; date of current version 2 August 2023. The work of Vasilii Voropaev and Vladimir Lazarev was supported by Russian Science Foundation under Grant 21-79-10325. The work of Shangran Xie was supported in part by the National Natural Science Foundation of China under Grant 62275021 and in part by Beijing Natural Science Foundation under Grant 4232078. *(Vasilii Voropaev and Shangran Xie contributed equally to this work.) (Corresponding author: Vladimir Lazarev.)*

Vasilii Voropaev and Daniil Batov are with the Science and Education Center for Photonics and IR-Technology, Bauman Moscow State Technical University, 105005 Moscow, Russia (e-mail: vladimir.al.lazarev@gmail.com; batov@bmstu.ru).

Shangran Xie was with the Max Planck Institute for the Science of Light, 91058 Erlangen, Germany. He is now with the School of Optics and Photonics, Beijing Institute of Technology, Beijing 100081, China (e-mail: sxie@bit.edu.cn).

Vladimir Lazarev is with the Science and Education Center for Photonics and IR-Technology, Bauman Moscow State Technical University, 105005 Moscow, Russia, and also with the Sechenov First Moscow State Medical University, 119991 Moscow, Russia (e-mail: vladimir.lazarev@bmstu.ru).

Mikhail Tarabrin is with the Science and Education Center for Photonics and IR-Technology, Bauman Moscow State Technical University, 105005 Moscow, Russia, and also with the Physical Institute of the Russian Academy of Sciences, 119991 Moscow, Russia (e-mail: tarabrinmk@bmstu.ru).

Aleksandr Donodin is with the Aston Institute of Photonic Technologies, Aston University, B4 7ET Birmingham, U.K. (e-mail: a.donodin@aston.ac.uk).

Johann Troles is with the Sciences Chimiques de Rennes, Université de Rennes I, 35042 Rennes, France (e-mail: johann.troles@univ-rennes1.fr).

Color versions of one or more figures in this article are available at https://doi.org/10.1109/JLT.2023.3253889.

Digital Object Identifier 10.1109/JLT.2023.3253889

I. Introduction

INFRARED supercontinuum (SC) sources [1], [2] have a wide range of applications such as high precision spectroscopy [3], molecule detection [4], optical clocks [5], [6], etc. SC generation has been obtained in various media pumped by different laser sources [7], [8], [9]. For instance, an SC spectrum covering 2 to 10 μm was obtained by pumping a planar waveguide by a bulk optical parametric oscillator at a wavelength of 4.2 μm [10].

At the same time, all-fiber versions of such sources are compact, stable, reliable, and easy to align, making them more promising for applications. One of the approaches that can be implemented in the all-fiber system is the use of SC generation in dispersion-shifted chalcogenide waveguides with an arsenic trisulfide (As_2S_3) core and a fused silica cladding [11], [12]. The main advantages of such waveguides are the high nonlinear coefficient as well as a simpler manufacturing technology [13] compared to planar waveguides [14]. As_2S_3 has a nonlinear refractive index two orders of magnitude higher than that of fused silica [15] and a wide transmission band in the wavelength range from 0.62 to 13 μm [16]. Despite the fact that the zero-dispersion wavelength (ZDW) of bulk As_2S_3 material locates at $\sim$ 4.9 μm [17], silica cladding can shift the ZDW of the hybrid waveguide to the operating range of the most common ultrafast silica-based fiber lasers (from 1 to 2.1 μm) by the contribution of waveguide dispersion.

SC in As_2S_3-silica waveguides was obtained in the range from 1.2 to 3.5 μm when pumped by a Cr:ZnS bulk laser at a wavelength of 2.35 μm [18]. Among studies with a fiber laser pump, SC (from 1 to 2 μm) in an As_2S_3-silica waveguide was obtained with an erbium-doped fiber laser at a wavelength of 1.55 μm [13]. A detailed study was carried out in As_2S_3-silica samples with different core diameters when pumped with an ultrafast erbium-doped ZBLAN fiber laser at a wavelength of 2.8 μm, the resulting SC covered the range from 1.1 to 4.8 μm [19]. Moreover, SC studies were carried out in such a structure with a core diameter of 1 μm using an ultrafast thulium-doped fiber laser [12], [20]. These works featured a dispersion wave predominantly generated in the spectral range from 3 to 4 μm. However, there have been no studies on the generation of SC pumped by thulium-doped fiber lasers in As_2S_3-silica waveguides with core diameters more than 1 μm, which leads to a different balance of nonlinear and dispersion effects during the

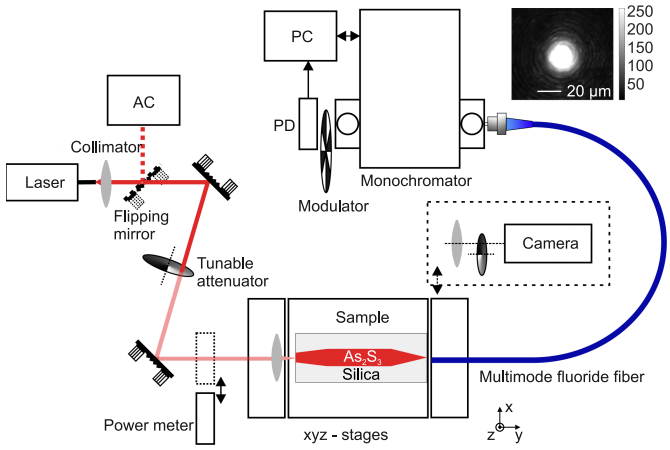

Fig. 1. Schematic of the experimental setup. PD, photodetector; PC, polarization controller; AC, autocorrelator.

formation of SC. Such a balance can provide SC spectra covering the entire 1–3 μm regime which are important for biomedical applications [21].

Thus, in this work, we report the generation of octave-spanning SC spectrum in As_2S_3-silica hybrid waveguides with core diameters of 1.2 μm and 1.7 μm pumped by a 78 fs ultrafast thulium-doped all-fiber master-oscillator power amplifier at 1.9 μm central wavelength. The refractive indices of As_2S_3 [17] and fused silica [22] at 1.9 μm wavelength are 2.428 and 1.440 respectively, indicating a high waveguide numerical aperture (1.96) and thus inefficient couplings at the input and output end-face. The nanospike (NS) structures are therefore integrated at the waveguide end-face to increase the coupling efficiency [12], [13]. The experiment revealed the generation of the third harmonic of the pump radiation, which influenced the formation of the SC. Compared with the previous work [23], the results reported here show SC spectra at different power levels along with a detailed description of theoretical modeling and the impact of the third harmonic generation process.

II. Experimental Configuration

A. Experimental Setup

Fig. 1 shows the schematic of the experimental setup. A home-made all-fiber ultrafast master oscillator power amplifier is used as the pump source (detailed description in [24]). The pump source consists of a thulium-doped fiber laser with hybrid mode-locking [25], a pulse stretcher, an amplifier based on a germanosilicate thulium-doped fiber with normal group velocity dispersion (GVD), and a large mode area fiber compressor. The emitted pulses have a central wavelength of 1.9 μm, a repetition rate of 23.84 MHz, and an average output power of 600 mW. Mechanical polarization controllers both in the laser and in the amplifier are used to adjust the pulse generation regime. Thus, with different settings of the polarization controllers, pulses at the amplifier output may be tuned from 65 fs to 1 ps, which is related to the dependence of the nonlinear refractive index on the polarization state of the radiation [26] and, as a consequence,

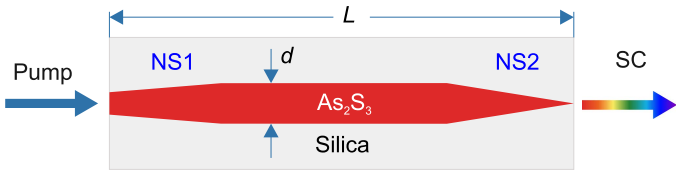

Fig. 2. The structure of the As_2S_3-silica hybrid waveguide. Two nanospikes are integrated at both waveguide ends.

to the different balance of dispersion and nonlinear effects in the amplifier and compressor (see in more detail in [24]). In the experiment, a pulse duration of 78 fs is used along with a maximum pulse energy of 25 nJ and a peak power of 200 kW.

The pump beam is firstly collimated using a 90-degree off-axis parabolic mirror along with a side path (switchable via a flipping mirror) directed to an autocorrelator, and then is coupled into the As_2S_3-silica hybrid waveguide using a 4-mm-focus lens (C036TME-D, Thorlabs, $T \approx 96\%$ at 1.9 μm). The output mode profile of the waveguide is monitored using a thermal CCD camera to optimize the in-coupling such that the near-field mode profile appears as single mode (top right inset of Fig. 1). The generated SC is collected by a multimode fluoride fiber with 200 μm core diameter which is transparent in the measured spectral range and is finally directed to the spectrometer. A monochromator along with a PbSe photodetector is used to collect data from 1 to 3 μm wavelength range. It has a diffraction grating with 300 lines per millimeter with a reciprocal linear dispersion of 17.2 nm/mm. The spectral resolution of the monochromator is set to 3.44 nm. A spectrometer with a diffraction grating and a CCD matrix is used for measurements in the wavelength range from 200 nm to 1000 nm.

B. Waveguides Parameters

The structure of the fabricated As_2S_3-silica hybrid waveguide is shown in Fig. 2. The length of the waveguide L is about 3 mm. The length of the input and output nanospikes is around 300 μm. The in-coupling efficiency of the hybrid waveguides is estimated to be 10%. The transmission of silica drops significantly in the wavelength range above 3 μm [27], [28]. Nevertheless, the losses of the fundamental mode in the developed waveguides do not exceed 1 dB/mm in the range from 620 nm to 4 μm [12], [19]. The manufacturing process of the hybrid waveguides was described in detail previously [13].

Due to the large difference in the refractive indices of the core and cladding, the fundamental radiation mode has a sufficiently strong electric field component along z -axis (directed along the optical axis of the waveguide). In this case, the scalar Schrödinger equation is used to model the propagation of the linearly polarized fundamental waveguide mode (see Appendix A). The vector field distribution of the mode is considered when calculating the mode nonlinear coefficient. The dispersion of fundamental waveguide mode ($\beta(\omega)$, where β is the propagation constant) is determined by analytically solving the eigenvalue equation of step-index waveguides [29], taking into account the wavelength dependencies of the refractive indices for As_2S_3 [17]

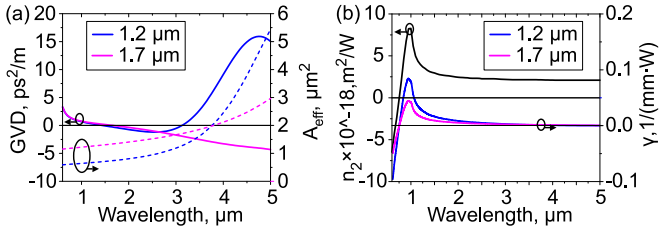

Fig. 3. (a) Calculated wavelength dependencies of GVD (solid, left axis) and effective areas (dashed, right axis) of the fundamental modes. (b) Dependence of the nonlinear refractive index n_2 of As_2S_3 on wavelength (black-solid, right axis). Nonlinear coefficient γ for both waveguides versus wavelength (left axis).

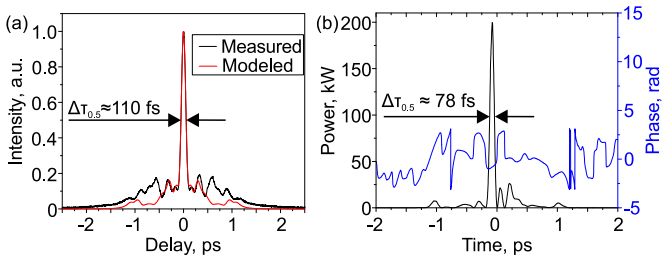

Fig. 4. (a) The measured and modeled autocorrelation trace of the pump pulse. (b) Power and phase distributions in time of the pump pulse in the SC model.

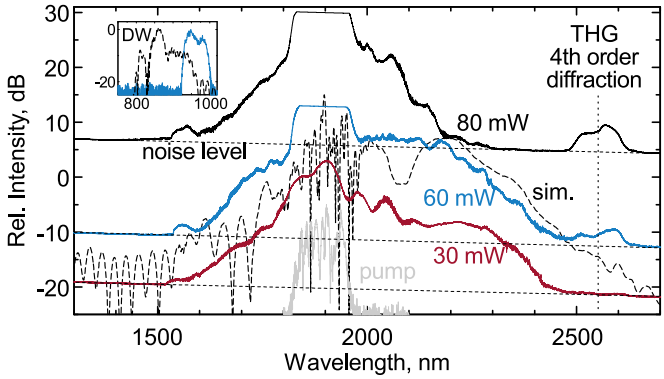

Fig. 5. Measured SC spectra at the output of the waveguide with a core diameter of 1.2 μm at different average pump powers before the coupling lens. The dashed lines show the numerical simulation results obtained by solving the nonlinear Schrödinger equation. The inset shows the measured spectrum around the dispersive wave (DW) under a pump power of 60 mW.

and fused silica [22]. Waveguides with core diameters of 1.2 μm and 1.7 μm are chosen for the experimental study based on the analysis of the parametric calculation of SC generation at different core diameters (see Appendix B). The calculated GVD for the hybrid waveguides with $d = 1.2$ μm and 1.7 μm are plotted as the solid lines in Fig. 3(a) (left axis). At the pump wavelength (1.9 μm), the GVD value is -0.6 ps^2/m and -0.25 ps^2/m for $d = 1.2$ μm and 1.7 μm respectively. The effective mode area of the fundamental mode is calculated as [1]:

$$A_{\text{eff}} = \frac{|\int(\mathbf{e}_\nu \times \mathbf{h}_\nu^*).\hat{z}dA|^2}{\int|(\mathbf{e}_\nu \times \mathbf{h}_\nu^*).\hat{z}|^2 dA}, \tag{1}$$

where $\mathbf{e}_\nu$ and $\mathbf{h}_\nu$ are the electric and magnetic fields, $\hat{z}$ is the unit vector along the fiber axis. The calculated dependencies of A_{eff} on wavelength are also shown in Fig. 3(a) (dashed lines, right axis).

Fig. 3(b) (black-solid line) shows the theoretical wavelength dependence of the nonlinear refractive index n_2 of As_2S_3 [30]. The n_2 value of As_2S_3 increases with increment of wavelength and changes the sign in the wavelength range from 600 nm to 1000 nm. Since SC is predominantly generated in the wavelength range of 1 μm to 3 μm in this work, consideration of the complex dependence is not required [31]. The nonlinear coefficient γ as a function of wavelength is calculated by the equation [1]:

$$\gamma = \frac{2\pi}{\lambda A_{\text{eff}}}\left(\frac{\epsilon_0}{\mu_0}\right)\frac{\int n^2(x,y)n_2(x,y)[2|\mathbf{e}_\nu|^4 + |\mathbf{e}_\nu^2|^2]dA}{3\int|(\mathbf{e}_\nu \times \mathbf{h}_\nu^*).\hat{z}|^2 dA}, \tag{2}$$

where ϵ_0 is vacuum permittivity, μ_0 is vacuum permeability, λ is wavelength. The resulting γ versus wavelength for both waveguides are also shown in Fig. 3(b) (right axis).

C. Pulse Characterization

The measured autocorrelation trace for pump pulses before coupling into the sample is shown in Fig. 4(a) (black). The SC simulation uses the power and phase temporal distributions of the pulse measured by the FROG method at other settings of the laser and amplifier polarization controllers (a detailed description of these measurements is given in [24]) and stretched in the time domain to the duration of the measured autocorrelation. The red curve (Fig. 4(a)) corresponds to the pulse autocorrelation obtained from the time distributions in Fig. 4(b). The FWHM pulse duration is about 78 fs.

Using a near-real field distribution and pulse phase allows us to analyze the effect of low-amplitude satellite pulses on the properties of the SC (spectral range and coherence). The differences when using a bandwidth-limited pulse with the same peak power and duration without satellite pulses are insignificant. Satellite pulses make almost no contribution to the spectral broadening and only add spectral intensity at the pump wavelength at the output of the waveguide.

III. Experimental and Simulation Results

A. Waveguide With $d = 1.2$ μm

Fig. 5 shows the measured SC spectra (solid curves) at the output of the waveguide for $d = 1.2$ μm hybrid waveguide. The grey curve is the measured spectrum of the pump source without coupling into the waveguide. At an average power of 30 mW (red-solid, corresponding to a peak power of 11 kW before coupling), the observed spectrum spans from 1.52 μm to 2.5 μm above the noise level, corresponding to a level of about -22 dB relative to the maximum value. When the average pump power is increased to 60 mW, the spectrum slightly broadens along with an enhanced emission at around 2.5 μm wavelength. That spectral component is confirmed to be originated from the 4th diffraction order of the third harmonic of the pump wave (see Appendix C). This indicates the increase in the radiation intensity of the third harmonic component (at 0.633 μm wavelength),

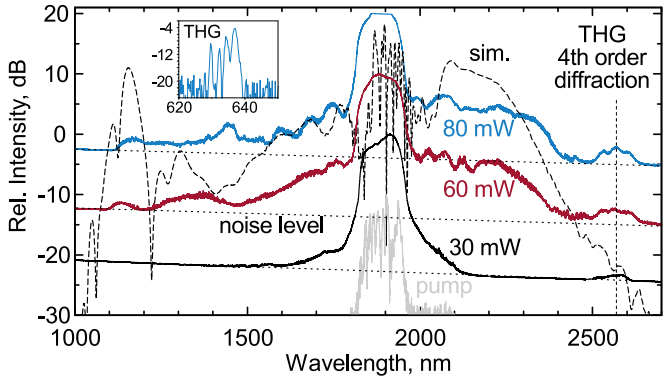

Fig. 6. Measured SC spectra at the output of waveguide with d = 1.7 μm at different average pump powers before the coupling lens. The dashed lines plot the numerical simulation results obtained by solving the nonlinear Schrödinger equation. The inset shows the measured spectrum around the third harmonic wavelength (THG) under a pump power of 80 mW.

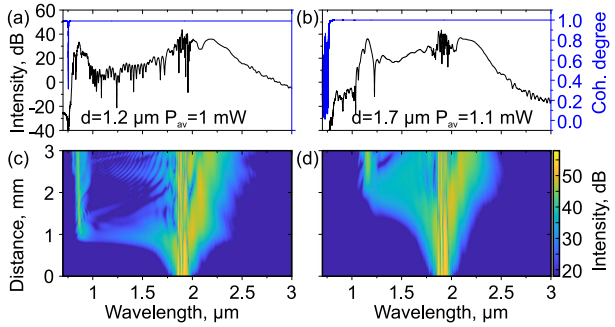

Fig. 7. (a) Simulated SC spectra (black) and its degree of coherence (blue) at the output end-face of hybrid waveguide when $d = 1.2$ μm and (b) $d = 1.7$ μm. (c) Evolutions of SC spectra along the waveguides with $d = 1.2$ μm and (d) 1.7 μm.

generated by the phase matching between the fundamental mode at the pump wavelength and the higher-order core mode at the third harmonic wavelength enabled by the large core-cladding index contrast [32]. The observed power saturation from 1.835 μm to 1.960 μm wavelength is associated with the pump beam coupling into the cladding mode. The dashed lines show the numerically simulated SC spectrum at 60 mW pump power level by solving the scalar nonlinear Schrödinger equation (see Appendix A). A spectral component at wavelength of 0.963 μm is also observed with the spectrometer (blue curve, inset of Fig. 5), which is roughly in agreement with the estimated emission wavelength of the dispersive wave. The discrepancy may be attributed by the variation of the waveguide dispersion due to thermal effects since the As_2S_3 core may be strongly heated by the absorption of the third harmonic component. The effect becomes even stronger at an average power of 80 mW. In this case, the peak of the third harmonic increases and the SC spectrum narrows down [33]. The waveguide is damaged when the pump power is further increased due to the absorption-induced heat. The critical pump power value for narrowing the supercontinuum spectrum can then be specified as 60 mW for this waveguide.

B. Waveguide With $d = 1.7$ μm

Fig. 6 shows the measured SC spectra (solid curves) at the output of the hybrid waveguide with a core diameter of 1.7 μm. At an average power of 30 mW, the spectrum is broadened spanning from 1.53 μm to 2.17 μm above the receiver noise level. At a power level of 60 mW, the spectrum spans from 1.09 μm to 2.5 μm at the receiver noise level, corresponding to a level of about -25 dB relative to the maximum value. At a power of 80 mW, the spectrum is similar to that of the 60 mW case. The inset plots show the measured third harmonic emission in the wavelength range from 0.63 μm to 0.64 μm recorded by the CCD spectrometer. The total power over this range can be estimated by integrating the spectrum and considering the collection efficiency (≈ 0.5 mW). Similar to the case of pumping of a waveguide with a core diameter of 1.2 μm, a strong spectral component is observed in the wavelength range from 2.5 μm to 2.6 μm at all pump powers, corresponding to the 4th order diffraction of the third harmonic of the pump radiation. Note that a larger core diameter (thus a smaller nonlinear coefficient) also induces a higher threshold for the spectrum narrowing effect for the $d = 1.7$ μm waveguide compared with the one with $d = 1.2$ μm.

C. Degree of Coherence

Fig. 7 shows the simulation results at a peak power of 341 W (corresponds to an average power of ≈ 10 mW in front of the coupling lens) for a sample with $d = 1.2$ μm (a and c) and 380 W (corresponds to an average power of ≈ 11 mW in front of the coupling lens) for a sample with $d = 1.7$ μm (b and d). The discrepancy between the experimental value of average power and the one used in the simulation may be attributed by the fact that the third harmonic generation process is not taken into account in the model. Fig. 7(a) and (b) show the emission spectra at at the waveguides outputs together with the spectral dependences of the coherence degrees (defined by (6) in Appendix A). Fig. 7(c) and (d) show the evolution of the spectrum along the length of the waveguides. It can be seen that the SC spectra at the output end of both waveguides are coherent in the entire spanning range. For both waveguides, the output radiation covers a range of more than one octave, making it possible to create an f-2f interferometer for stabilizing the carrier-to-envelope offset frequency of the radiation [34], [35].

IV. Discussion

When average power is increased to above 600 mW (peak power of 200 kW), both waveguides with $d = 1.2$ μm and $d = 1.7$ μm are presumably damaged due to heating associated with strong absorption of the third harmonic component by As_2S_3. An experiment is carried out with the same samples by pumping with a multi-soliton regime by tuning the polarization controller in another laser (a detailed description of which can be found in [36]). In this situation, at the same average power level, the peak power is reduced by 500 times due to the multi-pulse nature,

thus no third harmonic can be generated. It is found that none of the samples are damaged when the average pump power is increased to 700 mW [37]. This indicates that the damage of the waveguide is mainly induced by the peak power rather than the average power. The damage happens under the impact of the absorption of a strong third harmonic component generated in the waveguide.

Critical pump peak power at which the SC stops broadening for waveguides with core diameters greater than 1.7 μm can be estimated inversely proportional to the nonlinear coefficient. Thus, when modeling the generation of SC in waveguides with core diameters greater than 1.7 μm at the critical pump peak power there is no significant increase in the spectral range. However, this estimation of the critical power needs to be confirmed experimentally. It is also necessary to develop a mathematical model that takes into account the generation of the third harmonic generation and complex refractive index of As_2S_3.

V. Conclusion

We demonstrate experimentally and theoretically that an octave-spanning SC spectrum can be generated by pumping As_2S_3-silica hybrid waveguide with suitable core diameters by an all-fiber thulium-doped laser system. Numerical simulation shows that the generated SC spectrum is coherent and can be used to create an all-fiber coherent supercontinuum generator in the infrared region. The all-fiber laser source may be spliced with the As_2S_3-silica hybrid waveguide to form a full fiber-based mid-infrared SC source. The further broadening of the spectrum is currently limited by the third harmonic generation of pump light introducing strong absorption and thus damage of the As_2S_3 core.

Appendix A
Theoretical Model

The generalized nonlinear Schrödinger equation in the frequency domain is used to describe the supercontinuum generation process in samples in the following form [1]:

$$\frac{\partial \tilde{A}'}{\partial z} = i\gamma(\omega)\exp(-\hat{L}(\omega)z)\,\mathcal{F}\left\{A(z,t)\int_{-\infty}^{\infty} R(T')|A(z,T-T')|^2 dT'\right\}, \quad (3)$$

where $\tilde{A}' = \tilde{A}(z,\omega)\exp(-\hat{L}(\omega)z)$, $\hat{L}(\omega)$ is the linear operator, given by:

$$\hat{L}(\omega) = i(\beta(\omega) - \beta(\omega_0) - \beta_1(\omega_0)[\omega-\omega_0]) - \frac{\alpha(\omega)}{2}, \quad (4)$$

where $\alpha(\omega)$ is the frequency-dependent loss, $\beta(\omega)$ is the propagation constant, $\beta_1(\omega_0)$ is the first derivative of the propagation constant, ω_0 is the central angular frequency, $\tilde{A}(z,\omega)$ is the Fourier transform of the normalized amplitude $A(z,T)$ that $|A(z,T)|^2$ gives the instantaneous power in Watt, $\gamma(\omega)$ is the frequency-dependent nonlinear coefficient defined by (2), c is the speed of light in vacuum, ω is the angular frequency, $R(t)$ is the Raman response function, z is the distance in the waveguide, $T = t - \beta_1 z$ is the time in a co-moving frame at the envelope group velocity β_1^{-1}. Raman response function is defined as [1], [38]:

$$\begin{aligned} R(t) &= (1-f_R)\delta(t) + f_R h_R(t) \\ &= (1-f_R)\delta(t) + f_R\frac{\tau_1^2+\tau_2^2}{\tau_1\tau_2^2}\exp(-t/\tau_2)\sin(t/\tau_1)\Theta(t), \end{aligned} \quad (5)$$

where f_R represents the fractional contribution of the delayed Raman response to nonlinear polarization, $\Theta(t)$ is the Heaviside step function, $\delta(t)$ is the Dirac delta function, τ_1 is the period of vibrations, τ_2 is the dumping time of vibrations. We use $\tau_1 = 15.5fs$, $\tau_2 = 230.5fs$, $f_R = 0.1$ [12], [39]. Equation (3) is solved by the fourth-order Runge-Kutta method [1]. It is also revealed that the nonlinear refractive index of As_2S_3 strongly depends on the intensity of the incident light [15]. However, this dependence is not taken into account in this work, since the pulse intensities studied in our work are about 10 GW/cm^2, which is higher than the saturation intensity of the nonlinear refractive index ($\sim$ 1 GW/cm^2) [15].

The sensitivity of the SC to noise is estimated by calculating 100 SC spectra at different noises introduced into the pump radiation. Noise is defined as single photons at each considered emission frequency with a random phase (one photon per mode). Quantitative analysis of coherence is obtained by calculating the wavelength dependence of the modulus of the complex degree of first-order coherence, defined at each wavelength in the SC by [40]:

$$|g_{12}^{(1)}(\lambda, t_1 - t_2)| = \left|\frac{\langle \tilde{A}_1^*(\lambda,t_1)\tilde{A}_2(\lambda,t_2)\rangle}{\sqrt{\langle|\tilde{A}_1(\lambda,t_1)|^2\rangle\langle|\tilde{A}_2(\lambda,t_2)|^2\rangle}}\right|, \quad (6)$$

where angle brackets denote an ensemble average over independently generated pairs of SC spectra $[\tilde{A}_1(\lambda,t)\tilde{A}_2(\lambda,t)]$ obtained from a large number of simulations, and t is the time measured at the scale of the temporal resolution of the spectrometer used to resolve those spectra. Equation (6) is calculated at $t_1 - t_2 = 0$ corresponding to the fringe visibility at zero path difference in a double-slit experiment performed between independent SC spectra [41].

Appendix B
Optimization of the Waveguide Core Diameter

A parametric scanning is performed to determine the optimal core diameter for the generation of coherent SC in the wavelength range from 1 to 3 μm. The core diameter of the waveguide is varied from 1 to 3 μm with steps of 0.1 μm. The length of the waveguides in the calculation is set as 3 mm because at this length the emission spectrum is significantly broadened for each diameter of the core. The simulation use the nonlinear refractive index dependence shown in Fig. 3(b), which can be used in the region from 1 to 3 μm. The pump pulses in the model are in the form of a soliton and have a duration of 65 fs (the shortest duration achievable in a pump source [24]). The maximum power for each waveguide in the simulation is

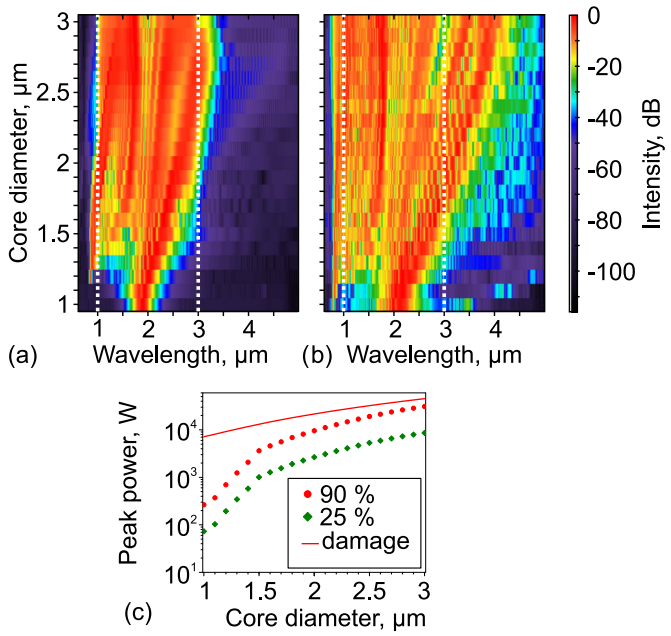

Fig. 8. Calculated spectra at the output of waveguides with different core diameters for a coupled 1.9 μm pump pulse of 65 fs duration and peak power equal to 25% (a) and 90% (b) of the maximum power at which no solution could be found in the model. (c) The peak powers used in the calculation and the estimated threshold of waveguide destruction.

estimated using the effective area of the waveguide mode and the measured damage threshold of As_2S_3 [42] and is shown by the red curve in Fig. 8(c). In each waveguide, when reaching a certain peak power a strong spectral component in the region of 750 nm begins to generate, corresponding to a change in the sign of the nonlinear refractive index (Fig. 3(b)). In this case, the calculation cannot be accurately performed and it is necessary to use another model [31]. Thus, for each waveguide, the maximum peak pump pulse power, at which the mathematical model is suitable and the calculation can be performed, is determined. Fig. 8 shows the results of the calculation for the values of peak power 25% (Fig. 8(a)) and 90% (Fig. 8(b)) of the maximum value at which the model works. The values of the peak power used in the simulation are shown in Fig. 8(c). At 90% maximum power, the spectrum covering the entire range from 1 to 3 μm is achieved in a waveguide with a core diameter of approximately 1.7 μm, so this core diameter is chosen for the experimental study. At core diameters from 1.7 to 3 μm, the spectrum begins to broaden in the spectral range from 3 to 4 μm. The waveguide with a diameter of 1.2 μm is chosen to experimental study the dynamics of changes in the width of the spectrum. All powers used in the simulation can be achieved using the developed pumping system [24].

Appendix C
Measurement of the Third Harmonic Component

The origination of the observed emission around 2.5 μm wavelength in Fig. 9 is validated by launching an emission at 635 nm wavelength (from a semiconductor laser) with an average power of 1 mW to the monochromator. The 2nd diffraction order at a wavelength of 1.27 μm is not observed in the

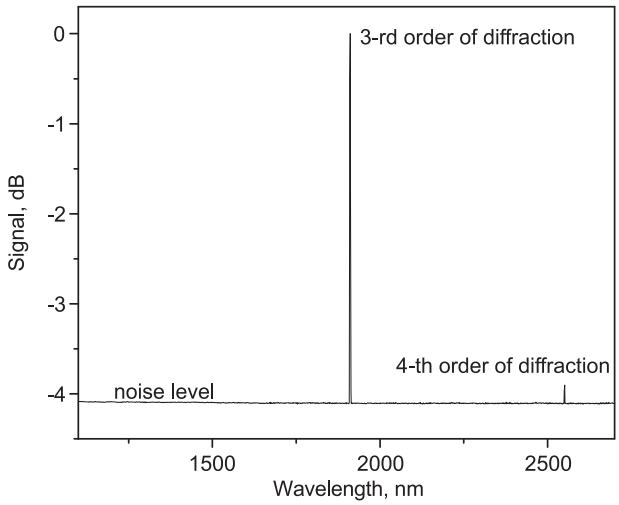

Fig. 9. The measured diffraction orders of the radiation at 635 nm wavelength.

measurement while the 3rd and 4th-orders are present, and the 3rd-order is 2.5 times stronger than the 4th one in intensity. The ratio of the detector sensitivity at a wavelength of 1900 nm to the sensitivity at a wavelength of 635 nm is 10.9, according to our measurements. Since the 3rd-order diffraction wavelength overlaps with the wavelength of the pump radiation, in which region the receiver is saturated by the residual pump beam in the cladding, only the 4th-order diffraction order is observed in the experiment.

Acknowledgment

The authors are grateful to Philip St. J. Russell for his endless enthusiasm, hours of fruitful discussions and the joy of scientific collaboration. Lazarev V. A. and Voropaev V. S. developed an experimental setup, conducted numerical modeling, and optimized the core diameter of the waveguide by simulation. Xie S. designed and fabricated waveguides and provided laser coupling into the fundamental mode of fabricated waveguides. The work of Lazarev V. A. and Voropaev V. S. was supported by the Russian Science Foundation under grant no. 21-79-10325. The work of Xie S. was supported by National Natural Science Foundation of China (No. 62275021) and Beijing Natural Science Foundation (No. 4232078).

References

[1] J. M. Dudley and J. R. Taylor, *Supercontinuum Generation in Optical Fibers*. Cambridge, U.K.: Cambridge Univ. Press, 2010.
[2] A. Schliesser, N. Picqué, and T. W. Hänsch, "Mid-infrared frequency combs," *Nature Photon.*, vol. 6, no. 7, pp. 440–449, 2012.
[3] N. Picqué and T. W. Hänsch, "Frequency comb spectroscopy," *Nature Photon.*, vol. 13, no. 3, pp. 146–157, 2019.
[4] C. Wang and P. Sahay, "Breath analysis using laser spectroscopic techniques: Breath biomarkers, spectral fingerprints, and detection limits," *Sensors*, vol. 9, no. 10, pp. 8230–8262, 2009.
[5] M. Gubin et al., "Femtosecond fiber laser based methane optical clock," *Appl. Phys. B*, vol. 95, no. 4, pp. 661–666, 2009.
[6] M. K. Tarabrin et al., "Application of the methane saturated dispersion resonance near 2.36 m over the temperature range of 77–300 K. for optical frequency standards," *J. Quantitative Spectrosc. Radiative Transfer*, vol. 177, pp. 241–247, 2016.

[7] T. S. Saini and R. K. Sinha, "Mid-infrared supercontinuum generation in soft-glass specialty optical fibers: A review," *Prog. Quantum Electron.*, vol. 78, 2021, Art. no. 100342.

[8] C. Lafforgueet al., "Supercontinuum generation in silicon photonics platforms," *Photon. Res.*, vol. 10, no. 3, pp. A43–A56, 2022.

[9] I. Zorin, P. Gattinger, A. Ebner, and M. Brandstetter, "Advances in mid-infrared spectroscopy enabled by supercontinuum laser sources," *Opt. Exp.*, vol. 30, no. 4, pp. 5222–5254, 2022.

[10] Y. Yu et al., "Experimental demonstration of linearly polarized 2–10 μm supercontinuum generation in a chalcogenide RIB waveguide," *Opt. Lett.*, vol. 41, no. 5, pp. 958–961, 2016.

[11] N. Granzow, S. P. Stark, M. A. Schmidt, A. S. Tverjanovich, L. Wondraczek, and P. S. Russell, "Supercontinuum generation in chalcogenide-silica step-index fibers," *Opt. Exp.*, vol. 19, no. 21, pp. 21003–21010, Oct. 2011. [Online]. Available: http://www.opticsexpress.org/abstract.cfm?URI=oe-19-21-21003

[12] N. Granzow et al., "Mid-infrared supercontinuum generation in As_2S_3-silica "nano-spike" step-index waveguide," *Opt. Exp.*, vol. 21, no. 9, pp. 10969–10977, May 2013. [Online]. Available: http://www.opticsexpress.org/abstract.cfm?URI=oe- 21-9-10969

[13] S. Xie et al., "As_2S_3-silica double-nanospike waveguide for mid-infrared supercontinuum generation," *Opt. Lett.*, vol. 39, no. 17, pp. 5216–5219, Sep. 2014. [Online]. Available: http://ol.osa.org/abstract.cfm?URI=ol-39-17-5216

[14] Q. Du et al., "Chip-scale broadband spectroscopic chemical sensing using an integrated supercontinuum source in a chalcogenide glass waveguide," *Photon. Res.*, vol. 6, no. 6, pp. 506–510, 2018.

[15] F. Smektala, C. Quemard, V. Couderc, and A. Barthélémy, "Non-linear optical properties of chalcogenide glasses measured by Z-scan," *J. Non-Crystalline solids*, vol. 274, no. 1–3, pp. 232–237, 2000.

[16] F. Vergeret al., "Surface enhanced infrared absorption (SEIRA) spectroscopy using gold nanoparticles on As_2S_3 glass," *Sensors Actuators B: Chem.*, vol. 175, pp. 142–148, 2012.

[17] W. S. Rodney, I. H. Malitson, and T. A. King, "Refractive index of arsenic trisulfide," *Josa*, vol. 48, no. 9, pp. 633–636, 1958.

[18] S. Xie et al., "Coherent octave-spanning mid-infrared supercontinuum generated in As_2S_3-silica double-nanospike waveguide pumped by femtosecond Cr:ZnS laser," *Opt. Exp.*, vol. 24, no. 11, pp. 12406–12413, May 2016. [Online]. Available: http://www.opticsexpress.org/abstract.cfm?URI=oe-24-11-12406

[19] P. Wang, J. Huang, S. Xie, J. Troles, and P. S. J. Russell, "Broadband mid-infrared supercontinuum generation in dispersion-engineered As_2S_3-silica nanospike waveguides pumped by 2.8 μm femtosecond laser," *Photon. Res.*, vol. 9, no. 4, pp. 630–636, 2021.

[20] K. F. Leeet al., "Midinfrared frequency combs from coherent supercontinuum in chalcogenide and optical parametric oscillation," *Opt. Lett.*, vol. 39, no. 7, pp. 2056–2059, 2014.

[21] D. C. Sordillo, L. A. Sordillo, P. P. Sordillo, L. Shi, and R. R. Alfano, "Short wavelengthinfrared optical windows for evaluation of benign and malignant tissues," *Proc. SPIE*, vol. 22, no. 4, 2017, Art. no. 045002.

[22] I. H. Malitson, "Interspecimen comparison of the refractive index of fused silica," *Josa*, vol. 55, no. 10, pp. 1205–1209, 1965.

[23] V. Voropaev et al., "Octave-spanning supercontinuum generated in As_2S_3-Silica waveguides pumped by Tm-doped all-fibre MOPA," in *Proc. Conf. Lasers Electro- Opt. Europe Eur. Quantum Electron. Conf.*, 2021, pp. 1–1.

[24] V. Voropaev et al., "All-fiber ultrafast amplifier at 1.9 μm based on thulium-doped normal dispersion fiber and LMA fiber compressor," *Sci. Rep.*, vol. 11, no. 1, 2021, Art. no. 23693, doi: 10.1038/s41598-021-02934-4.

[25] A. Donodin et al., "Numerical model of hybrid mode-locked Tm-doped all-fibre laser," *Sci. Rep.*, vol. 10, no. 1, 2020, Art. no. 17396, doi: 10.1038/s41598-020-74194-7.

[26] S. Chernikov and J. Taylor, "Measurement of normalization factor of n_2 for random polarization in optical fibers," *Opt. Lett.*, vol. 21, no. 19, pp. 1559–1561, 1996.

[27] R. Kitamura, L. Pilon, and M. Jonasz, "Optical constants of silica glass from extreme ultraviolet to far infrared at near room temperature," *Appl. Opt.*, vol. 46, no. 33, pp. 8118–8133, 2007.

[28] S. T. Yang et al., "Comparing the use of mid-infraredversus far-infrared lasers for mitigating damage growth on fused silica," *Appl. Opt.*, vol. 49, no. 14, pp. 2606–2616, 2010.

[29] A. W. Snyder and J. Love, *Optical Waveguide Theory*. London, U.K.: Chapman Hall, 1983.

[30] R. Rangel-Rojo et al., "Near-infrared optical nonlinearities in amorphous chalcogenides," *Opt. Commun.*, vol. 109, no. 1–2, pp. 145–150, 1994.

[31] J. Bonetti, N. Linale, A. D. Sánchez, S. M. Hernández, P. I. Fierens, and D. F. Grosz, "Photon-conserving generalized nonlinear schrödinger equation for frequency-dependent nonlinearities," *JOSA B*, vol. 37, no. 2, pp. 445–450, 2020.

[32] G. P. Agrawal, *Nonlinear Fiber Optics 5th Edition*. Cambridge, MA, USA: Academic Press, 2013.

[33] W. Gaoet al., "Visible light generation and its influence on supercontinuum in chalcogenide As_2S_3 microstructured optical fiber," *Appl. Phys. Exp.*, vol. 4, no. 10, 2011, Art. no. 102601.

[34] A. Apolonski et al., "Controlling the phase evolution of few-cycle light pulses," *Phys. Rev. Lett.*, vol. 85, pp. 740–743, Jul. 2000. [Online]. Available: https://link.aps.org/doi/10.1103/PhysRevLett.85.740

[35] V. Yakovlev et al., "Phase-stabilized 4-FS pulses at the full oscillator repetition rate for a photoemission experiment," *Appl. Phys. B*, vol. 76, no. 3, pp. 329–332, 2003.

[36] V. Voropaev et al., "Generation of multi-solitons and noise-like pulses in a high-powered thulium-doped all-fiber ring oscillator," *Sci. Rep.*, vol. 9, no. 1, pp. 1–11, 2019.

[37] A. Donodin et al., "Supercontinuum generation in a As_2S_3-Silica nanospike waveguide pumped by Tm-doped fiber laser," in *Proc. Conf. Lasers Electro- Opt. Europe Eur. Quantum Electron. Conf.*, 2019, pp. 1–1.

[38] K. J. Blow and D. Wood, "Theoretical description of transient stimulated Raman scattering in optical fibers," *IEEE J. Quantum Electron.*, vol. 25, no. 12, pp. 2665–2673, Dec. 1989.

[39] C. Xiong et al., "Characterization of picosecond pulse nonlinear propagation in chalcogenide As_2S_3 fiber," *Appl. Opt.*, vol. 48, no. 29, pp. 5467–5474, 2009.

[40] G. Genty, S. Coen, and J. M. Dudley, "Fiber supercontinuum sources," *JOSA B*, vol. 24, no. 8, pp. 1771–1785, 2007.

[41] X. Gu et al., "Experimental studies of the coherence of microstructure-fiber supercontinuum," *Opt. Exp.*, vol. 11, no. 21, pp. 2697–2703, 2003.

[42] C. You et al., "Mid-infrared femtosecond laser-induced damages in As_2S_3 As_2Se_3 chalcogenide glasses," *Sci. Rep.*, vol. 7, no. 1, pp. 1–9, 2017.